

# Thermohydraulic Performance Optimization of Solar Air Heater via Tailored Inverted L-Shaped Rib: A CFD Investigation

Sayed Tanvir Ahmed,<sup>a)</sup> Tripta Sarker,<sup>b)</sup> and Ratul Das<sup>c)</sup>

*Department of Mechanical Engineering, Shahjalal University of Science and Technology, Sylhet-3114, Bangladesh.*

<sup>a)</sup>Corresponding author: sytanvir.mech@gmail.com

<sup>b)</sup>triptasarker@gmail.com

<sup>c)</sup>ratuldas.9052@gmail.com

**Abstract.** The solar air heater is a thermohydraulic equipment that increases convective heat transfer by artificially roughening the absorber plate with repeated ribs. In this study, 2-D Computational Fluid Dynamics (CFD) observation is done to analyze the properties of heat transfer and fluid flow friction of an artificially roughed Solar Air Heater (SAH) with inverted L-shaped ribs of varying thickness of relative roughness ( $0.2 \leq t/e \leq 0.8$ ). The roughness parameters such as the thickness of relative roughness ( $0.2 \leq t/e \leq 0.8$ ), the height of relative roughness ( $0.021 \leq e/D \leq 0.042$ ), the pitch of constant relative roughness ( $P/e = 7.14$ ) and Reynolds number ( $3800 \leq Re \leq 18000$ ) are varied for the analysis. The impact of the thickness of relative roughness on the Thermohydraulic Performance Parameter (*THPP*) (Overall energy performance) is investigated in the study. Governing equations with RNG  $k-\epsilon$  turbulence model are solved using ANSYS FLUENT. The contours of velocity, pressure, turbulent kinetic energy, and turbulent intensity are represented pictorially to understand the flow physics clearly. The study found that Nusselt Number (*Nu*), flow friction factor (*f*), and Thermohydraulic Performance Parameter (*THPP*) are greatly influenced by rib configurations. A maximum *THPP* of 1.69 is obtained using the rib configuration of *t/e* of 0.8 and *e/D* of 0.042.

## INTRODUCTION

A solar air heater is a specialized apparatus intended to use solar energy for the purpose of heating air. The system comprises a collector, absorber, and duct system that collaborate to capture sunlight and elevate the temperature of the air flowing through. Widely utilized in home and commercial settings, its primary functions include providing heat to areas and raising the temperature of ventilation air. Integrating solar air heaters into existing heating systems can reduce reliance on conventional energy sources, leading to lower costs and a smaller environmental impact. Solar air heaters are employed in the agricultural and industrial domains to accelerate the dehydration of crops, grains, and other commodities.

Smooth solar air heaters are inferior in heat transfer owing to the low coefficient of heat transfer. This is because laminar sublayers resist heat transmission in smooth ducts. But artificially roughening causes an increase in friction factor. If roughness is used only at the wall of the solar air heater, turbulence intensity will increase only close to the wall. This breaks the laminar sublayer and improves the coefficient of heat transfer considerably with a relatively lower friction factor. The use of artificial roughness hence has a great influence on heat transmission. Thermohydraulic performance parameters (*THPP*) which are calculated from Nusselt number and friction factor is greatly impacted by the installation of artificial roughness.

At the very beginning, Prasad et al. [1] used artificial roughness to the solar air heater using diagonal wire rib at the heat transfer surface. In this experimental study, the insertion of rib results in 14% thermal enhancement over smooth duct.

After this study, a wide range of experimental and numerical investigations have been done on the design and shape optimization of ribs. Chamfered rib roughness was examined experimentally by Karwa et al. [2] and found 2 times improvement in Stanton number across the smooth duct. Another work of similar shape with grooved rib with compound turbulator was experimentally examined by Layek et al. [3] and identified 3.78 times friction factor (*f*) and 3.24 times Nusselt number (*Nu*) improvement. Lanjewar et al. [4] experimentally examined W-shaped rib roughness and found friction factor 2.01 times and Nusselt number 2.36 times improved. Kumar et al. [5] experimentally investigated multi-V-shaped rib along with gap and Improved friction factor 6.12 and Nusselt number 6.32 times. Pandeya et al. [6] found a 4.96 times increase over plain duct both for friction factor (*f*) and Nusselt number (*Nu*) using multiple ribs of arch shape. Ravi and Saini [7] studied on solar air heater using a double pass where assembly of V-shaped and stagger rib roughness was used. Pungentet et al. [8] studied on punched winglet. Thermal enhancement

improves by a factor of 2.17 in this study. A study by Baissi et al. [9] used a delta-shaped vortex generator to investigate the thermal performance and found at roughness height  $e = 6$  and  $Re = 11,382$ , the heat transmission performance is 2.26 times smooth plate.

Gawande [10] experimentally and numerically investigated an inverted L-shaped rib where the pitch of relative roughness and height of relative roughness were varied. There are various scopes of increasing thermohydraulic performance by modifying the design parameters of the inverted L shape. Investigation on the cross-section thickness of the inverted L-shaped rib has not been done yet.

In this study, a novel parameter is suggested called thickness of relative roughness ( $t/e$ ) where  $t$  is the cross-section thickness of the inverted L-shaped rib. The objectives of this paper are given below:

- To examine the impact of the novel parameter thickness of relative roughness ( $t/e$ ) on Nusselt number ( $Nu$ ), average flow friction factor ( $f$ ), and thermohydraulic performance parameter ( $THPP$ ).
- To obtain the configuration with optimal  $THPP$  to study the overall effect of thickness of relative roughness under the same pumping power constraint.

Optimum rib geometry was found from a total of nine rib configurations. An energy study has been done with thermal parameters. Contours of pressure, velocity, turbulent kinetic energy, and intensity are pictorially presented for a better understanding of flow physics.

## CFD INVESTIGATION

The Artificially roughed 2D solar air heater with inverted L-shaped with varying thickness was numerically studied to observe heat transfer and frictional loss. ANSYS Fluent 2022 R1 was used for this computational analysis. Based on the assumptions mentioned below the numerical model was developed.

1. 2-D steady state heat transfer and fluid flow.
2. Single-phase flow, turbulent flow, and incompressible through the duct.
3. Thermally and hydrodynamically fully developed flow.
4. Constant thermo-physical characteristics for absorber and air plate.
5. Constant heat flux and negligible radiation heat transfer.

## CFD Domain Description

The conventional method of analysis of a rectangular three-dimensional solar air heater is the numerical 2D investigation to reduce computational time and cost [11]. The Chaube et al. [12] study's two-dimensional computational domain is analogous to this study and is shown in Fig. 1. Three sections were created in the domain using ANSYS ICEM CFD named Entrance segment ( $L_1 = 245$  mm), Test segment ( $L_2 = 280$  mm), and Exit segment ( $L_3 = 115$  mm). The entry segment is used for flow to be fully developed right before going into the test segment. The duct aspect ratio is kept at 5 ( $W/H$ ) where height ( $H$ ) is 20 mm and width ( $W$ ) is 100 mm. The equivalent diameter ( $D$ ) was 33.33 mm. The domain length used in this study was recommended by ASHAR standard 93 - 2003 [13].

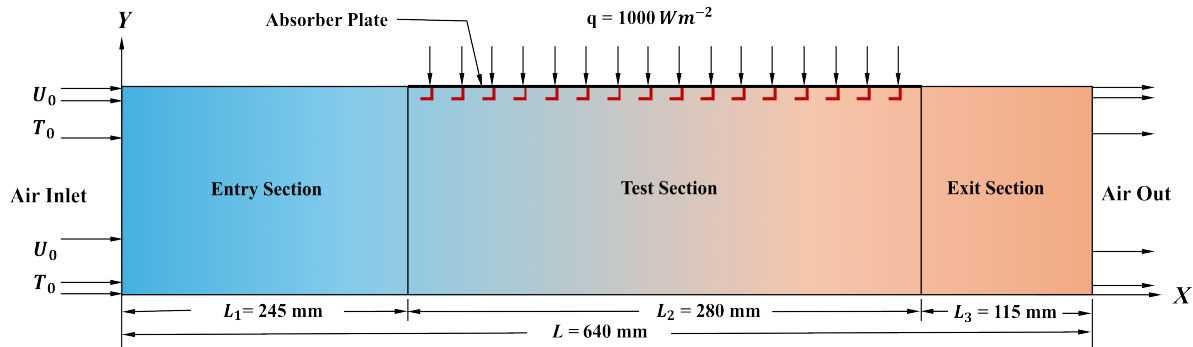


**FIGURE 1.** 2-D computational region.

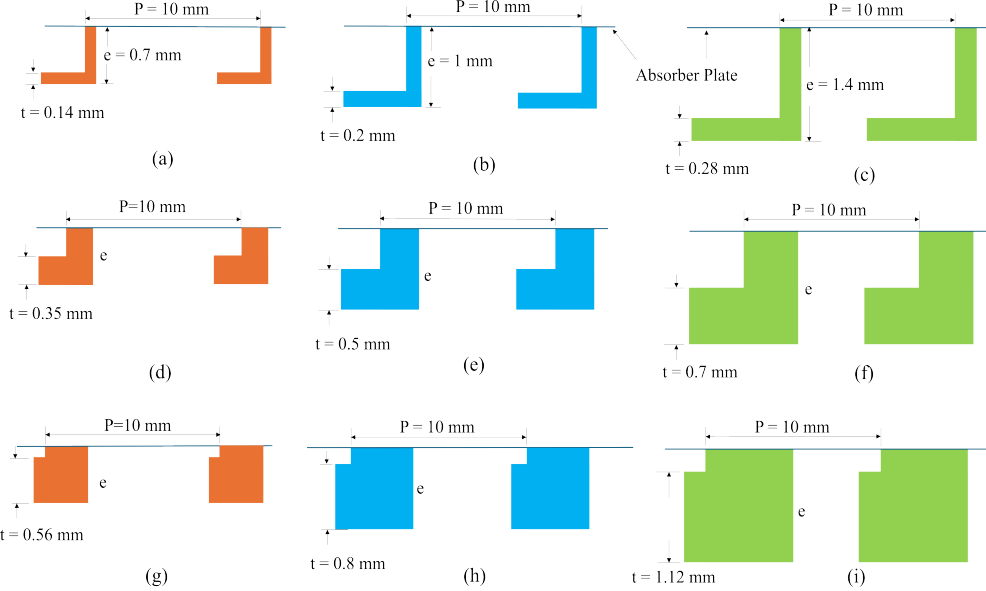


**FIGURE 2.** Schematic of different configurations of inverted L-shaped rib with the thickness of relative roughness ( $t/e$ ) of 0.2, 0.5, and 0.8 and height of relative roughness ( $e/D$ ) of 0.021, 0.03 and 0.042.

In this study thickness of relative roughness ( $t/e$ ) of inverted L-shaped rib by varying the cross-section thickness of shape in terms of ratio of 0.2, 0.5, and 0.8 was carried out. Ribs were attached to the inner surface of the test segment's top wall. Other surfaces were considered smooth surfaces. Constant  $1000 \text{ W m}^{-2}$  heat flux ( $\dot{q}$ ) was employed on the upper surface of the test section's top wall. In this study, a constant pitch of 10 mm is kept between the ribs as 10 mm gives better THPP in most solar air heaters.

Three rib heights of 0.7 mm, 1 mm, and 1.4 mm were considered, and corresponding heights of relative roughness ( $e/D$ ) were 0.042, 0.03, and 0.021. Reynolds number ranges between 3800 to 18000 and 6 discrete values were taken. For considering the laminar sub-layer properly an exquisite mesh was generated near the walls. In Table 1, the geometry and operating parameters are listed.

**TABLE 1.** Dimensional and operating variables.

Parameters and Ranges	Symbols	Span
Entry segment	$L_1$	245 mm
Test segment	$L_2$	280 mm
Exit segment	$L_3$	115 m
Hydraulic diameter	$D$	33.33 mm
Duct depth	$H$	20 mm
Width of the duct	$W$	100 mm
Rib height	$e$	1.4mm, 1mm, 0.7mm
L shape thickness	$t$	0.14mm - 1.12mm
Duct aspect-ratio	$W/H$	5
Pitch of relative roughness	$e/P$	7.14 (Fixed)
Height of relative roughness,	$e/D$	0.042, 0.030, 0.021
Relative roughness thickness	$t/e$	0.2, 0.5, 0.8
Reynolds number	$Re$	3800-18000
Prandtl number	$Pr$	0.7

## Governing Equations

In solar air heaters, thermal and flow of fluid analysis can be done by the CFD method. To solve pressure and velocity fields, mass and momentum equations were used and for solving temperature fields, energy conservation equation were used with species transport equation. The equations are as stated:

Continuity equation:

$$\frac{\partial(\rho u_i)}{\partial x_i} = 0 \quad (1)$$

Momentum Equation:

$$\frac{\partial}{\partial x_j}(\rho u_i u_j) = -\frac{\partial p}{\partial x_i} + \frac{\partial}{\partial x_j} \left[ \mu \left( \frac{\partial u_i}{\partial x_j} + \frac{\partial u_j}{\partial x_i} \right) \right] + \frac{\partial}{\partial x_j}(-\rho \bar{u}_i' u_j') \quad (2)$$

Energy Equation:

$$\frac{\partial}{\partial x_i}(\rho u_j T) = \frac{\partial}{\partial x_j} \left( (\Gamma + \Gamma_t) \frac{\partial T}{\partial x_j} \right) \quad (3)$$

Where the thermal diffusivity of molecules is  $\Gamma$  and  $\Gamma_t$  is the thermal diffusivity of turbulence respectively and are presented by the Eqn. (4),

$$\Gamma = \frac{\mu}{Pr} \quad \Gamma_t = \frac{\mu_t}{Pr_t} \quad (4)$$

Eqn. (1) and Eqn. (2) are also stated as Reynolds average Navier stock equation. The term  $-\bar{\rho}(\bar{u}_i' u_j')$  in Eqn. (2) represent the effect of turbulence. The governing equation was converted into a system of algebraic equations which was solved numerically. ANSYS Fluent 2022 R1 uses the FVM code to transform the governing equations into algebraic equations and solve them numerically.

## Grid Generation

The structured grid was constructed with ANSYS ICEM CFD 22.1. To capture the laminar sublayer and velocity gradient to the boundary properly, a very fine mesh was generated and kept  $y+$  value less than 1. The boundary layer mesh element size was 0.1mm and gradually increased up to the centerline of the duct using linear spacing. The aspect ratio was between 1-3 and the orthogonality was 1. These grid parameters ensure the mesh is of high quality.

The refined mesh throughout the domain is shown in Fig. 3(a) and near the L-shaped region is shown in Fig. 3(b). In this study, the total number of elements was 245827.

## Boundary Condition

For the analysis, air was used as the working fluid and assumed to have constant thermal properties at 300 K throughout the duct. Boundary condition was created in ANSYS ICEM CFD at different edges of the region. At the entrance, boundary condition was applied as velocity, and air entered at 300K at uniform velocity ( $U_0$ ) corresponding to the Reynolds number. At the outlet face, the pressure outlet was adopted. On the test region's upper wall fixed heat flux ( $\dot{q}$ ) condition was applied. The rest of the walls are kept in adiabatic condition. All walls are under no-slip condition. Thermal properties used in the study are shown in Table 2.

## Selection of Appropriate Turbulence Model

Solar air heaters deal with turbulent flows. The selection of models should be appropriate turbulence model to capture turbulence occurrence. In this study, the RNG  $k-\varepsilon$  model was chosen to examine heat transfer and fluid

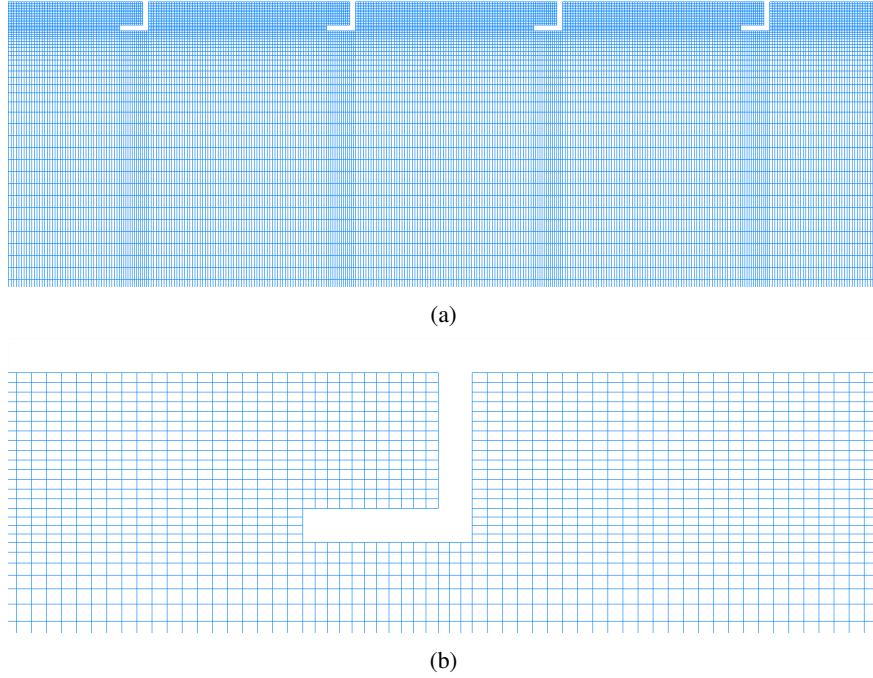


**FIGURE 3.** Structured grid of computational region constructed using ANSYS ICEM CFD.

flow properties. Using this model Yadav and Bhagoria [14] found results for smooth duct which is very close to the correlations (empirical) of Blasius and the Dittus–Boelter of solar air heater. The turbulence  $k$ - $\varepsilon$ (RNG) model employs several equations to extract the kinetic turbulence energy  $k$  and the rate of dissipation  $\varepsilon$ .

$$\frac{\partial}{\partial x_i} (\rho k U_i) = \frac{\partial}{\partial x_j} \left( \alpha_k \mu_{eff} \frac{\partial k}{\partial x_i} \right) + G_k - \rho \varepsilon \quad (5)$$

$$\frac{\partial}{\partial x_i} (\rho \varepsilon u_j) = \frac{\partial}{\partial x_j} \left( \alpha_k \mu_{eff} \frac{\partial k}{\partial x_i} \right) - C_{1\varepsilon} \frac{\varepsilon}{k} (G_k) - C_{2\varepsilon} \rho \frac{\varepsilon^2}{k} - R_\varepsilon \quad (6)$$

### Solution Method

The RNG k-epsilon model is used, and the energy equation is kept on. Used hydraulic diameter to calculate input and outflow boundary conditions and Reynolds number. Air is taken as working fluid and thermal characteristics are kept constant. Inlet velocity and turbulence intensity are calculated from Eqn. (9) and Eqn. (10). Applying the upwind biased scheme of second order, each equation is discretized by FVM and solved in a segregated manner with FVM using ANSYS FLUENT 2022 R1. The SIMPLE algorithm used and coupled pressure velocity suggested by Patankar [15]. For energy and momentum equation convergence criteria were set to  $10^{-6}$  and the rest of was  $10^{-3}$ . Values of the coefficient of heat transfer and pressure difference were extracted from post-processing.

### Data Reduction for CFD Analysis

The impact of the thickness of relative roughness ( $t/e$ ) of the L-shaped (inverted) rib underside of the top wall of SAH with a fixed pitch of 10mm on Nusselt number, friction factor, and  $THPP$  were investigated. The average

**TABLE 2.** Thermo-physical properties at 300K of absorber and Air.

Properties	Absorber	Air
Thermal Conductivity, ' $C_p$ ' J·kg $^{-1}$ ·K $^{-1}$	202.4	0.0242
Density, ' $\rho$ ' kg·m $^{-3}$	2719	1.225
Specific Heat, ' $k$ ' J·kg $^{-1}$ ·K $^{-1}$	1006.43	871
Viscosity, ' $\mu$ ' Pa·s	1.7894e-05	-

Nusselt number for roughed SAH was calculated using Eqn. (7),

$$Nu = \frac{hD}{k} \quad (7)$$

Where  $h$  demonstrates the heat convection coefficient and calculated average friction factor using Eqn. (8).

$$f = \frac{(\Delta P/l)D}{2\rho U^2} \quad (8)$$

Where  $\Delta P$  is the pressure difference of the test section. The Reynold number is calculated using Eqn. (9).

$$Re = \frac{\rho UD}{\mu} \quad (9)$$

Where  $D$  is the equivalent diameter. The turbulent intensity at the core is calculated using Eqn. (10) for the fully developed flow, developed by ANSYS 2004.

$$I = 0.16Re^{-1/8} \quad (10)$$

Thermal Hydraulic Performance Parameter (*THPP*) used for calculation of heat transfer enhancement respected to frictional loss. This relation was suggested by Webb and Eckert [16] and Lewis [17] and given by Eqn. (11).

$$THPP = \frac{Nu_r/Nu_s}{(f_r/f_s)^{1/3}} \quad (11)$$

*THPP*'s value should be greater than one. The empirical correlation of Nusselt number ( $Nu_s$ ) for the plain duct was developed by Dittus–Boelter [18] and given by Eqn. (12).

$$Nu_s = 0.023Re^{0.8}Pr^{0.4} \quad (12)$$

Empirical Correlation of friction factor ( $f_s$ ) was developed for smooth duct developed by Blasius [19] and given by Eqn. (13).

$$f_s = 0.0791Re^{-0.25} \quad (13)$$

**TABLE 3.** Grid sensitivity analysis.

Element number	Nusselt number, ( $Nu$ )	Deviation, (%)	Friction factor, ( $f$ )	Deviation, (%)
141257	99.021	—	0.0258	—
201154	100.112	1.089779	0.0281	8.9147
245827	100.544	0.429662	0.0279	0.7117
325453	100.547	0.002983	0.0277	0.7168
404199	100.5489	0.001889	0.0276	0.3610

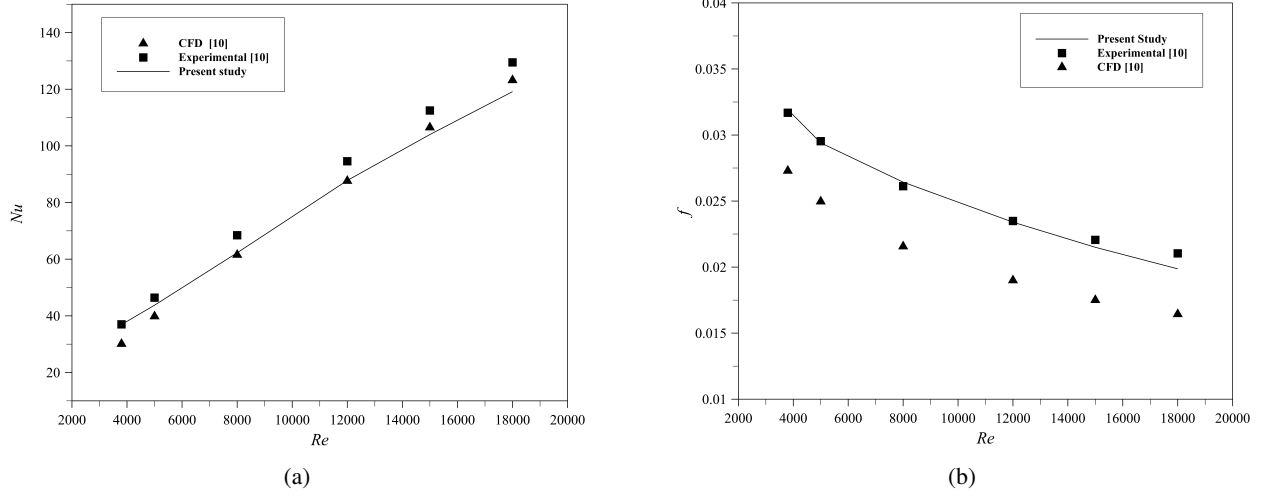


**FIGURE 4.** Validation of current study with the CFD and experimental study [10]. (a)  $Nu$  and (b)  $f$ .

### Grid Independence Test

The grid independence test was carried out with 5 different element numbers for friction factor ( $f$ ) and Nusselt number ( $Nu$ ). Table 3 shows that for element numbers greater than 245,000, the Nusselt number shows very little deviation. For element numbers above 200,000, the friction factor deviation also stays below 1%. As a result, element numbers of approximately 245,000 were maintained throughout the CFD analysis to provide accurate and reliable results without unnecessarily raising computational costs.

### Validation of the Present Study

The current investigation was substantiated with the experimental and CFD investigation executed by Gawande et al [10] where Fig. 4(a) depicts the Nusselt number comparison and the friction factor comparison is depicted in Fig. 4(b). The current study's friction factor ( $f$ ) and Nusselt number ( $Nu$ ) exhibit good agreement with the results of the experiment and CFD. The average error between the experimental and present study was found around 1.8% for friction factor and 6.2% for Nusselt number. This confirms the accuracy and method's reliability of the present study.

## RESULT AND DISCUSSION

### Heat Transfer Characteristics

Figure 5 depicts Reynolds number as a function, variation of Nusselt ( $Nu$ ) number is influenced by the relative thickness ratio ( $t/e$ ) at fixed  $e/D$  ratio. With an increase of  $t/e$  average Nusselt number increases considerably. The reason is rib attachment area increases with the plate. The same heat must now be released through the relatively lower area. On the other hand,  $Re$  causes a rise in the average  $Nu$ . Fig. 5(a-c) depict that the alteration of the Nusselt number also depends on the height of relative roughness. As roughness ( $e/D$ ) increases Nusselt number increases. An increase in rib height causes the laminar sublayer to break which advances to development of heat transfer. Additionally, the height of relative roughness decreases the attachment area at the inner side of the absorber plate, which leads to an improvement in heat transfer.

The average Nusselt number is lower at the low Reynolds number and close to the smooth duct. At a low Reynolds number, laminar sub-layer is dominant and rib height cannot catch it properly. Hence at low  $Re$  heat transfer resistance is high.

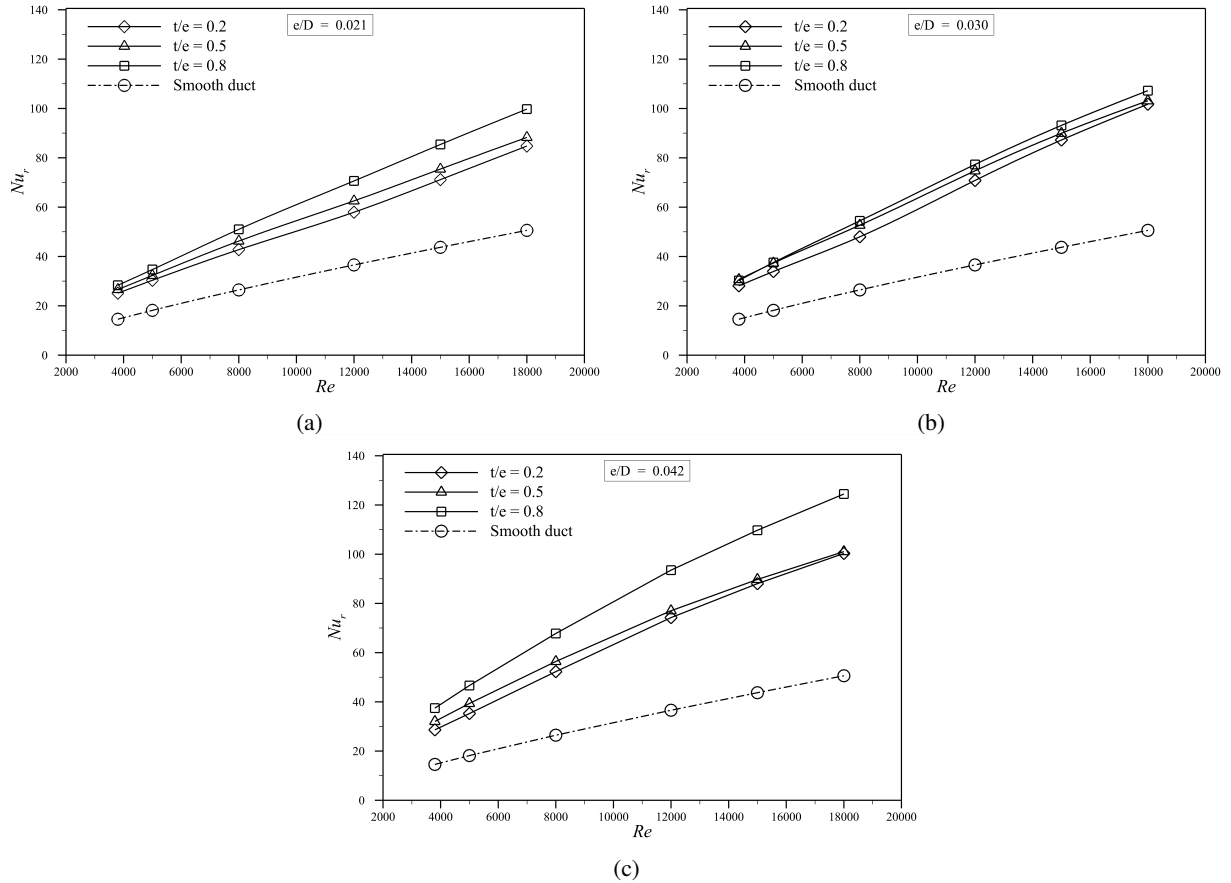


**FIGURE 5.** Variation of average Nusselt number ( $Nu$ ) for distinct values of roughness thickness ( $t/e$ ) at roughness height ( $e/D$ ) of (a) 0.021, (b) 0.030 and (c) 0.042.

As turbulent intensity increases convection coefficient of heat transfer increases. Turbulent intensity increases with  $Re$  and roughness height. As  $Re$  increases turbulent intensity and turbulent kinetic energy increase resulting in a higher average Nusselt number. It can be distinguished from the contour that turbulent intensity and kinetic energy are higher adjacent to rib walls depicted in Fig. 7 and Fig. 8, consecutively. Breaking of the laminar sublayer causes vortex generation near the rib areas which leads to higher turbulent intensity and kinetic energy. Nusselt number enhancements are higher than the smooth duct for all cases.

## Flow Friction Characteristics

The influence of height ( $e/D$ ) and thickness( $t/e$ ) of relative roughness and the range of  $Re$  on friction factor are depicted in Fig. 6. Friction factor is highest at  $e/D = 0.42$  at 3800 Reynolds and the lowest friction factor is at  $e/D = 0.021$  at  $Re = 18000$  depicted in Fig. 6(c) and Fig. 6(a) respectively. It is also seen that ( $t/e$ ) has no impact on the friction factor.

As Reynolds number increases the laminar sublayer suppresses and reduces its thickness and the velocity gradient normal to the plate reduces. Hence pressure drop reduction results in a lower friction factor at a higher Reynolds number. However, at low Reynolds numbers, laminar characteristics are dominant at the boundary which causes a higher friction factor.

The height of relative roughness has a major influence on the friction factor. At a higher ( $e/D$ ), the rib fully breaks the laminar sublayer and flow separation occurs. A low-pressure zone develops behind the rib, which causes a greater factor of friction in contrast to that of the smooth duct. As roughness height ( $e/D$ ) reduces laminar sublayer breaks partially and flow separation is lower resulting in a lower friction factor. In this study friction factor is highest and

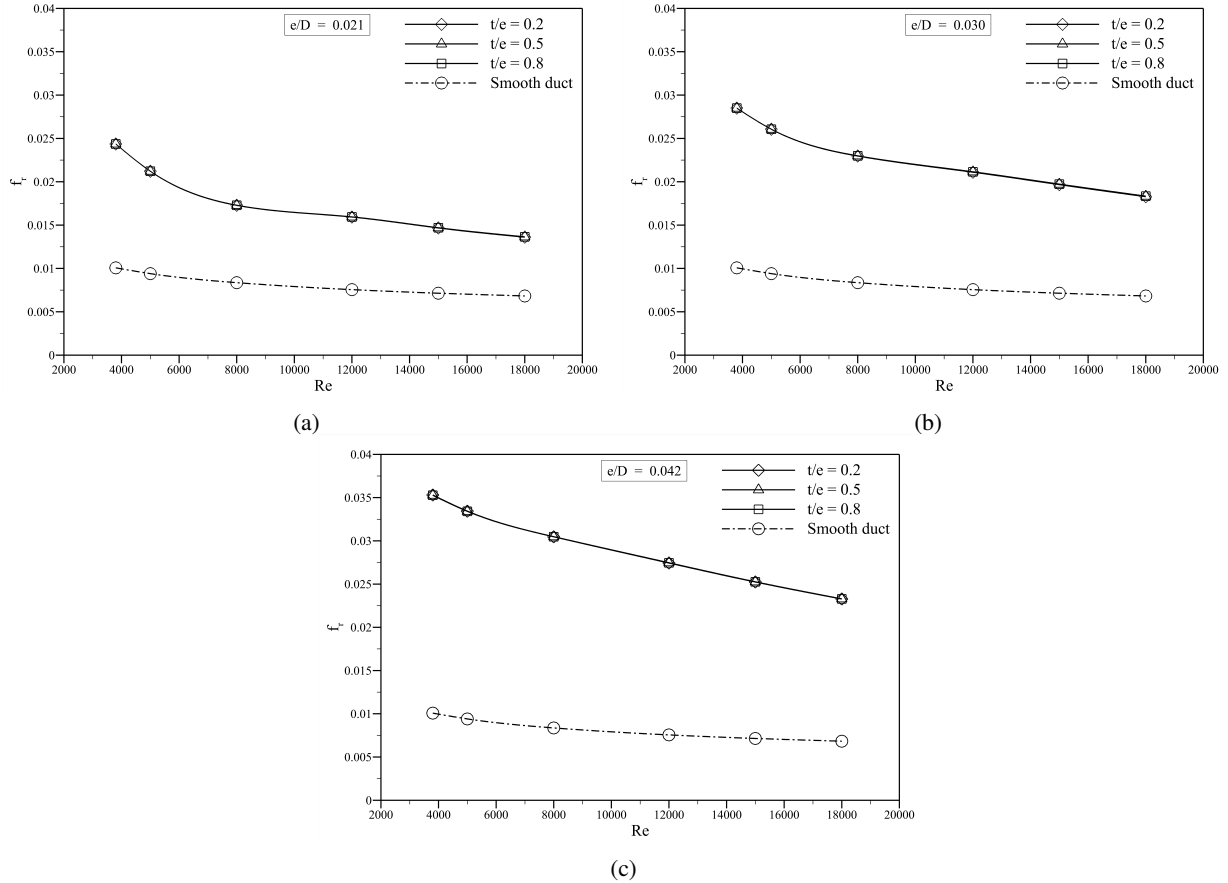


**FIGURE 6.** Variability of friction factor  $f$  for distinct values of roughness thickness ( $t/e$ ) at roughness height ( $e/D$ ) of (a) 0.021, (b) 0.030 and (c) 0.042.

lowest at 0.042 and 0.021 height of relative roughness respectively as rib height changes.

The thickness of relative roughness ( $t/e$ ) has a minor effect on the friction factor. As thickness ( $t$ ) is varied with constant height of relative roughness ( $e/D$ ), rib height is also constant. The capturing of the laminar sublayer remains persistent regardless of variations in thickness. When the thickness ( $t$ ) varies while the rib height ( $e$ ) remains constant, a similar low-pressure zone develops for three different relative roughness thicknesses ( $t/e$ ). Hence friction factor is almost similar for the thickness of relative roughness ( $t/e$ ). The height of relative roughness affects the turbulent intensity and kinetic energy. At higher heights of relative roughness turbulent intensity and turbulent kinetic energy are greater which leads to in higher friction factor.

**TABLE 4.** Thermohydraulic Performance Parameter (THPP) obtained by CFD at different value of  $t/e$  and  $e/D$ .

$e$ (mm)	$e/D$	$P$ (mm)	$t$ (mm)	$t/e$	$Re = 3800$	$Re = 5000$	$Re = 8000$	$Re = 12,000$	$Re = 15,000$	$Re = 18,000$
0.7	0.021	10	0.14	0.2	1.285	1.275	1.27	1.236	1.281	1.331
			0.35	0.5	1.36	1.357	1.373	1.333	1.357	1.386
			0.56	0.8	1.448	1.458	1.514	1.506	1.536	1.565
1	0.03	10	0.2	0.2	1.364	1.329	1.296	1.375	1.423	1.448
			0.5	0.5	1.487	1.464	1.423	1.45	1.467	1.467
			0.8	0.8	1.468	1.472	1.47	1.5	1.519	1.525
1.4	0.042	10	0.28	0.2	1.292	1.272	1.285	1.321	1.322	1.318
			0.7	0.5	1.447	1.42	1.386	1.37	1.347	1.327
			1.12	0.8	1.692	1.683	1.666	1.663	1.648	1.635

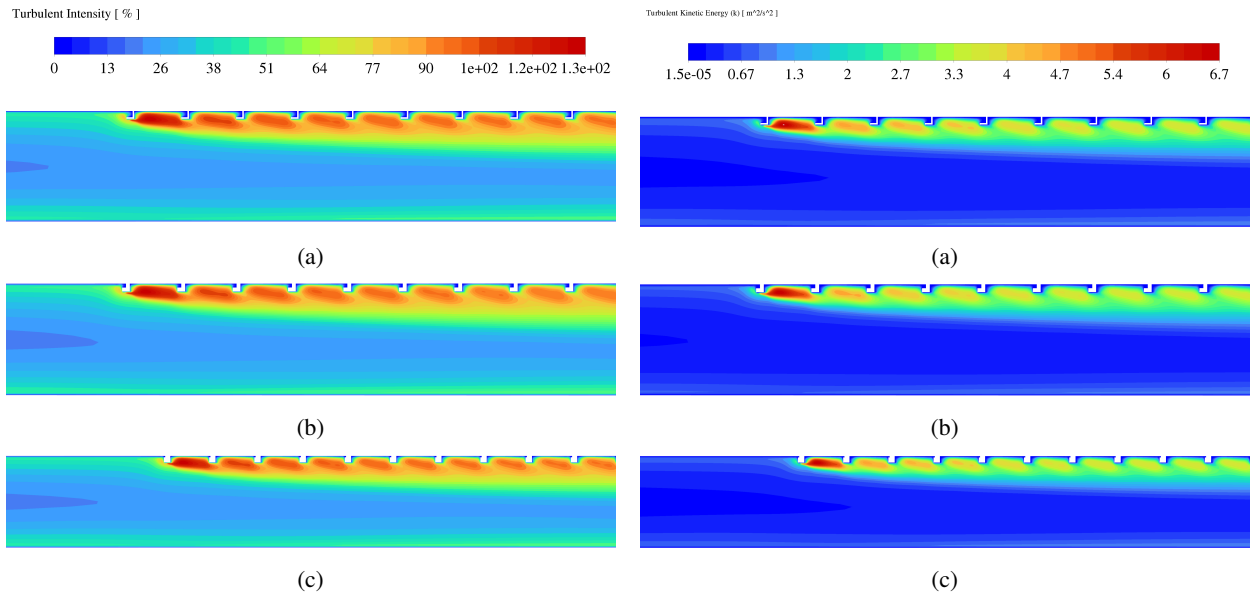


**FIGURE 7.** Turbulent intensity contour for (a)  $t/e = 0.2$ , (b)  $t/e = 0.5$ , and (c)  $t/e = 0.8$ .

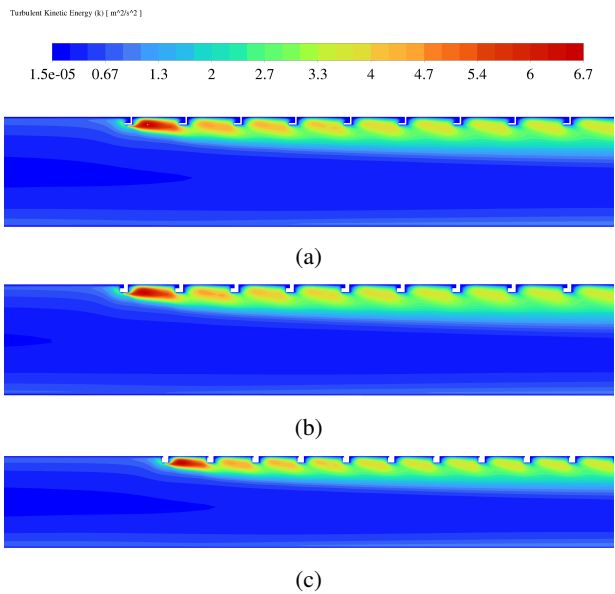


**FIGURE 8.** Kinetic energy contour for (a)  $t/e = 0.2$ , (b)  $t/e = 0.5$ , and (c)  $t/e = 0.8$ .

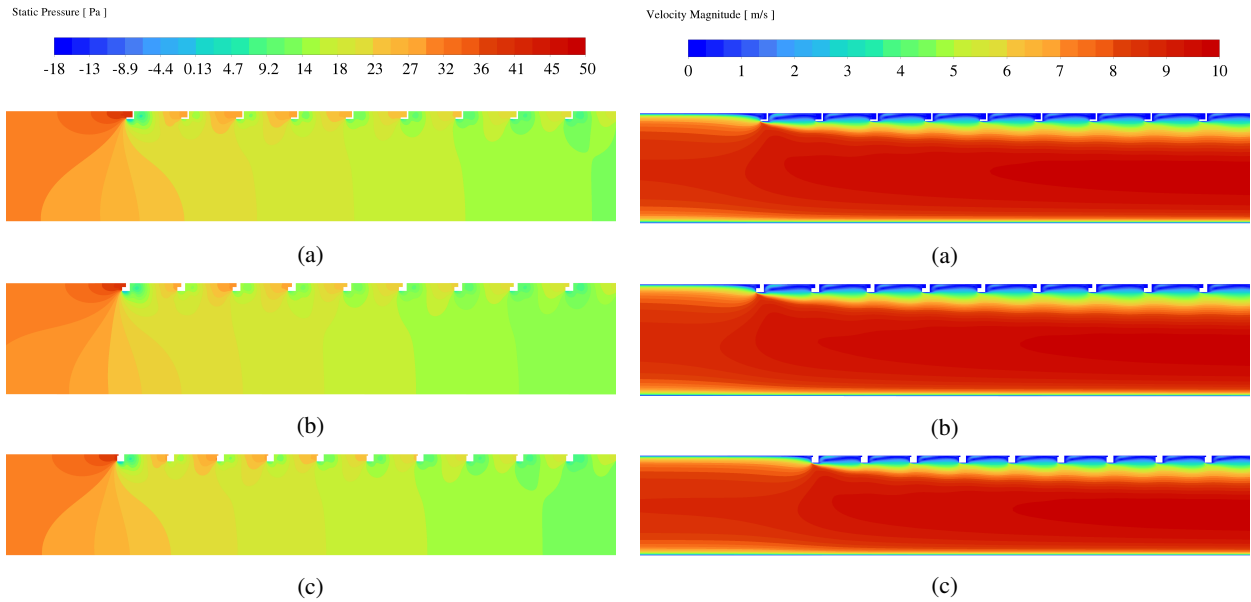


**FIGURE 9.** Pressure contour at  $Re = 18000$  for (a)  $t/e = 0.2$ , (b)  $t/e = 0.5$ , and (c)  $t/e = 0.8$ .

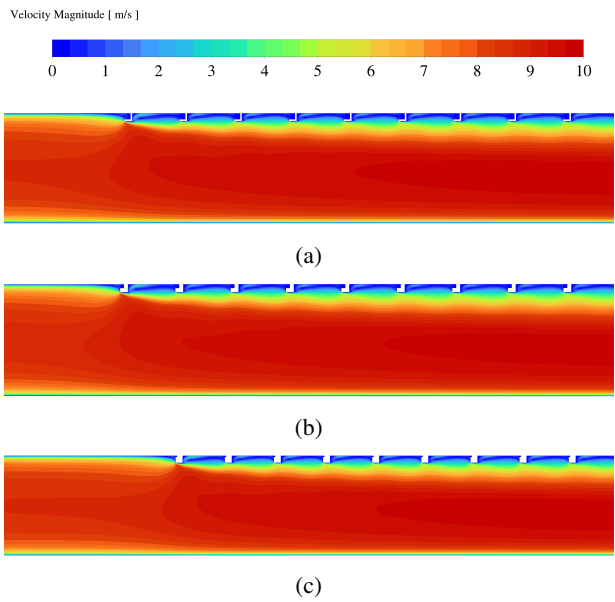


**FIGURE 10.** Velocity contour at  $Re = 18000$  for (a)  $t/e = 0.2$ , (b)  $t/e = 0.5$ , and (c)  $t/e = 0.8$ .

## Thermohydraulic Performance Parameter (THPP)

Thermohydraulic performance parameters of this investigation are depicted in Fig. 11 and revealed the influence of  $(e/D)$  and  $(t/e)$  on THPP. Maximum THPP is found at a height of relative roughness of 0.042 and at the thickness of relative roughness( $t/e$ ) of 0.8 for each Reynolds number as shown in Fig. 11(c). It has been revealed that THPP varied between 1.28 to 1.7 for the span of investigated parameters. It is found that  $(t/e) = 0.8$  at  $e/D = 0.042$  is the best among all combinations at the Re of 3800.

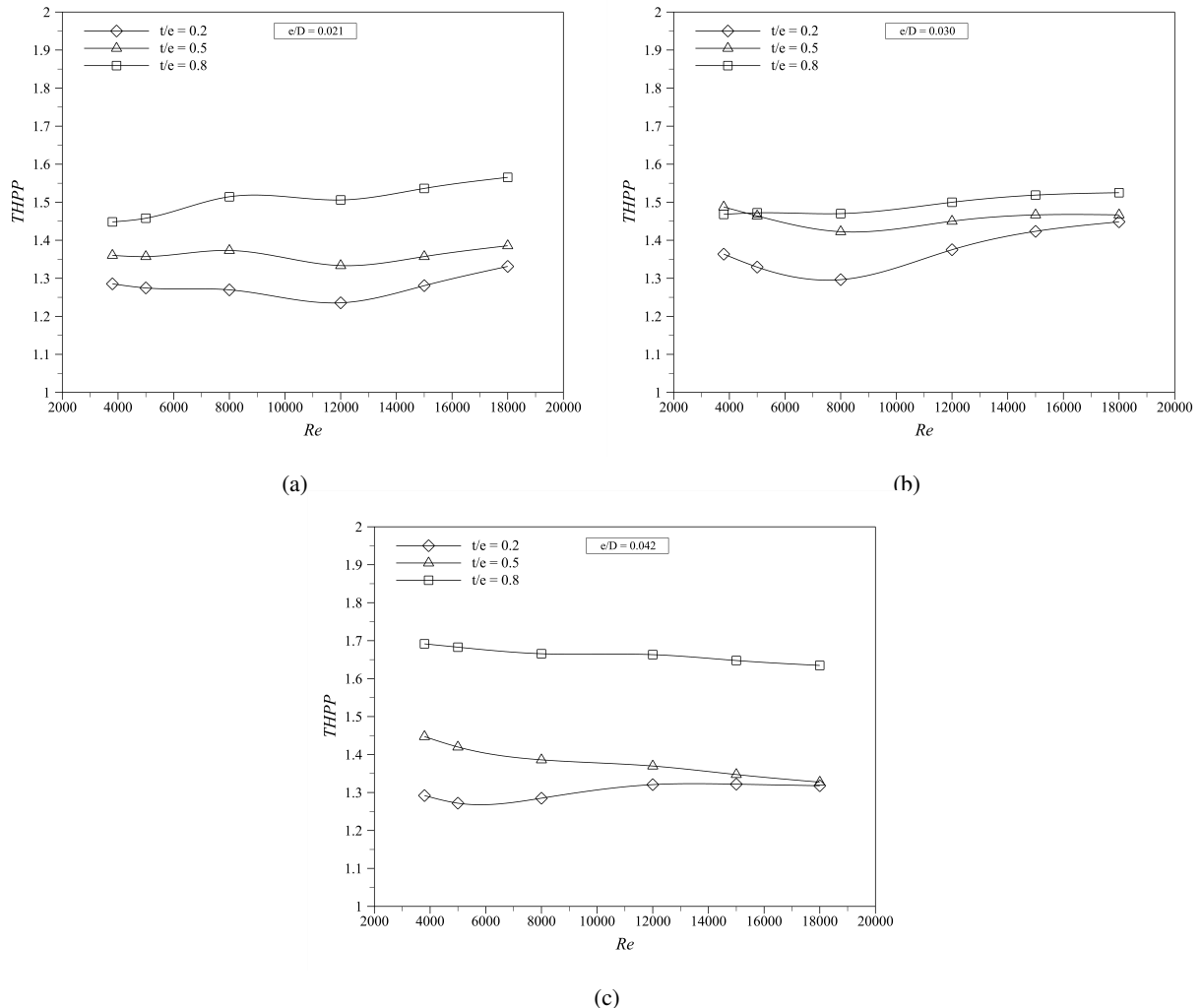


**FIGURE 11.** Thermohydraulic Performance Parameter  $THPP$  variation with Reynolds numbers for varied roughness values thickness ( $t/e$ ) at different ( $e/D$ ) of (a) 0.021, (b) 0.030 and (c) 0.042.

## CONCLUSION

In this study, A computation incorporating CFD was performed on a two-dimensional solar air heater with L-shaped (inverted) ribs attached to the undersurface of the absorbing plate. The impact of a novel design parameter named thickness of relative roughness( $t/e$ ) on Nusselt number, average friction factor, and thermohydraulic performance parameter ( $THPP$ ) was studied. The key findings are stated below:

- Average Nusselt number increases with the increase of Renolds number. Nusselt number increases with the increase of the thickness of relative roughness ( $t/e$ ).
- Maximum Nusselt number is 2.46 times over the unobstructed duct when the thickness of relative roughness is 0.8 and the height of relative roughness is 0.042.
- A Decrease in Reynolds number causes a decrease in the average friction factor. The thickness of the relative roughness has a negligible effect on the friction factor.
- The  $THPP$  range between 1.235 to 1.691 for the range of parameters studied.
- The optimum configuration was obtained by evaluating the best thermohydraulic performance parameter ( $THPP$ ) of 1.691 at the thickness of relative roughness and height of 0.8 and 0.042 respectively.

## REFERENCES

1. K. Prasad and S. Mullick, "Heat transfer characteristics of a solar air heater used for drying purposes," *Applied Energy* **13**, 83–93 (1983).
2. R. Karwa, "Thermo-hydraulic performance of solar air heaters having integral chamfered rib roughness on absorber plates," *Energy* **26**, 161–176 (2001).
3. A. Layek, J. Saini, and S. Solanki, "Heat transfer and friction characteristics for artificially roughened ducts with compound turbulators," *International Journal of Heat and Mass Transfer* **50**, 4845–4854 (2007).
4. A. Lanjewar, J. Bhagoria, and R. Sarviya, "Heat transfer and friction in solar air heater duct with W-shaped rib roughness on absorber plate," *Energy* **36**, 4531–4541 (2011).
5. A. Kumar, R. Saini, and J. Saini, "Experimental investigation on heat transfer and fluid flow characteristics of air flow in a rectangular duct with Multi v-shaped rib with gap roughness on the heated plate," *Solar Energy* **86**, 1733–1749 (2012).
6. N. Pandey, V. Bajpai, and Varun, "Experimental investigation of heat transfer augmentation using multiple arcs with gap on absorber plate of solar air heater," *Solar Energy* **134**, 314–326 (2016).
7. R. K. Ravi and R. Saini, "Experimental investigation on performance of a double pass artificial roughened solar air heater duct having roughness elements of the combination of discrete multi V shaped and staggered ribs," *Energy* **116**, 507–516 (2016).
8. P. Promvonge and S. Skullong, "Enhanced heat transfer in rectangular duct with punched winglets," *Chinese Journal of Chemical Engineering* **28**, 660–671 (2020).
9. M. Baissi, A. Brima, K. Aoues, R. Khanniche, and N. Moummi, "Thermal behavior in a solar air heater channel roughened with delta-shaped vortex generators," *Applied Thermal Engineering* **165**, 113563 (2020).
10. V. B. Gawande, A. Dhole, D. Zodpe, and S. Chamoli, "Experimental and CFD investigation of convection heat transfer in solar air heater with reverse L-shaped ribs," *Solar Energy* **131**, 275–295 (2016).
11. A. Singh Yadav and J. Bhagoria, "Numerical investigation of flow through an artificially roughened solar air heater," *International Journal of Ambient Energy* **36**, 87–100 (2015).
12. A. Chaube, P. Sahoo, and S. Solanki, "Analysis of heat transfer augmentation and flow characteristics due to rib roughness over absorber plate of a solar air heater," *Renewable Energy* **31**, 317–331 (2006).
13. A. S. Yadav and J. Bhagoria, "A CFD based thermo-hydraulic performance analysis of an artificially roughened solar air heater having equilateral triangular sectioned rib roughness on the absorber plate," *International Journal of Heat and Mass Transfer* **70**, 1016–1039 (2014).
14. S. V. Patankar, *Numerical Heat Transfer and Fluid Flow*, 1st ed. (CRC Press, 2018).
15. W. H. McAdams, T. K. Sherwood, and R. L. Turner, "Heat Transmission From Condensing Steam to Water in Surface Condensers and Feedwater Heaters," *Transactions of the American Society of Mechanical Engineers* **48**, 1233–1258 (1926).
16. A. Standard, "Standard 93-2003 "methods of testing to determine the performance of solar collectors"," ASHRAE, Atlanta (2003).
17. R. Webb and E. Eckert, "Application of rough surfaces to heat exchanger design," *international journal of heat and mass transfer* **15**, 1647–1658 (1972).
18. M. Lewis, "Optimising the thermohydraulic performance of rough surfaces," *international Journal of Heat and Mass transfer* **18**, 1243–1248 (1975).
19. P. J. Pritchard and J. W. Mitchell, *Fox and McDonald's introduction to fluid mechanics* (John Wiley & Sons, 2016).